PERGAMON

International Journal of Heat and Mass Transfer 42 (1999) 1327–1341

International Journal of HEAT and MASS TRANSFER

Control of Marangoni–Bénard convection

Haim H. Bau*

Department of Mechanical Engineering and Applied Mechanics, University of Pennsylvania, Philadelphia, PA 19104-6315, U.S.A.

Received 17 February 1998; in final form 23 June 1998

Abstract

It is demonstrated that the critical Marangoni number for transition from the no-motion (conduction) to the motion state in the Marangoni–Bénard problem of an infinite fluid layer heated from below and cooled from above can be increased through the use of feedback control strategies effecting small perturbations in the boundary data.

Nomenclature

The appropriate dimensions accompany dimensional quantities. All other quantities are nondimensional.

a wave number, $a=\sqrt{k_x^2+k_y^2}$
C_p specific heat at constant pressure [kJ kg^{-1} K^{-1}]
d liquid layer's height [m]
D differential operator $D=\mathrm{d}/\mathrm{d}z$
g gravitational acceleration [m s^{-2}]
H curvature of the free interface
k thermal conductivity [W m^{-1} K^{-1}]
k_x, k_y wave numbers in the x and y directions
K controller gain
n normal unit vector
N amplitude of surface deformation
p pressure
S surface tension
t time
T dimensional temperature [K]
x, y horizontal Cartesian coordinates
z vertical coordinate
$\mathbf{u}$ velocity vector
u, v, w velocity components in the x, y, z directions
W vertical velocity amplitude.

Greek symbols

β the opposite of the vertical temperature gradient [K m^{-1}]
Γ stress tensor
η location of the free surface
θ nondimensional temperature
θ' nondimensional temperature's deviation from its conductive value
Θ temperature amplitude
$\kappa=k/\rho C_p$ thermal diffusivity
ν kinematic viscosity [m^2 s^{-1}]
ρ density [kg m^{-3}]
σ growth rate
τ tangent vector.

Subscripts

A atmosphere
c critical
I imaginary part
F free surface
R real part
r relative
w solid surface.

Superscripts

* denotes dimensional quantities. The same quantities without the (*) are nondimensional.

Nondimensional groups

$Bi=hd/k$ Biot number
$Bo=\rho g d_f^2/S_0^*=gd_f^3/\nu\kappa\, C$ Bond number
$C=\rho\nu\kappa/S_0^* d$ crispation number
$F=gd^3/\nu\kappa$ Galileo number
$M=(-\mathrm{d}S^*/\mathrm{d}T)\beta d^2/\rho\nu\kappa$ Marangoni number
$Pr=\nu/\kappa$ Prandtl number.

* Tel.: 001 215 898 8363; Fax: 001 215 573 6334; E-mail: bau@eniac.seas.upenn.edu

0017–9310/98/$ - see front matter
PII: S0017–9310(98)00234–8

1. Introduction

The ability to control complex convective flow patterns is important in both technology and fundamental science. In many technological processes, the naturally occurring flow patterns may not be the optimal ones. By controlling the flow, one may be able to optimize the process. The ability to stabilize otherwise nonstable states may also assist one in gaining deeper insights into the dynamics of flows.

In prior experimental and theoretical investigations [1–5], it was demonstrated that through the use of linear and nonlinear control strategies, chaotic convection in a thermal convection loop could be suppressed. Similarly, Tang and Bau [6–12], Tang [13], and Howle [13–15] have shown that the critical Rayleigh number for the onset of convection in the Rayleigh–Bénard problem can be significantly delayed. For example, Tang and Bau [10, 12] microfabricated arrays of thermal actuators on the heated surface. The actuators modified the heated surface's temperature or heat flux in proportion to the deviation of measured interior temperatures from desired, conductive values. With this control strategy, they were able to maintain a no-motion state under conditions when, in the absence of a controller, motion would occur. In this paper, a similar control strategy is applied to stabilize the no-motion state of the Marangoni–Bénard problem. Although other actuation methods are possible and may provide better performance than the thermal actuation, the thermal actuation was chosen for study because it is relatively easy to implement in practice [10].

The problem of suppressing cellular convection in the Marangoni–Bénard problem has attracted some interest in the literature. Or and Kelly [16, 17] used open loop control and proposed delaying the onset of cellular convection in the Marangoni–Bénard problem by causing the fluid in the layer to oscillate slowly about a zero mean with out-of-phase, two horizontal velocity components. Recently, Or et al. [18] studied theoretically the use of the feedback control strategies similar to those proposed by Tang and Bau [6–12] in the Rayleigh–Bénard problem to stabilize long wavelength instabilities in the Marangoni–Bénard convection. They also utilized a nonlinear control similar to the one employed by Yuen and Bau [4] in the thermal convection loop problem to render the subcritical bifurcation supercritical.

In this paper, I utilize a linear controller to delay the onset of instability. The analysis is valid for all wavelengths and it takes into account bifurcations both into time-independent and oscillatory modes. The objective of the controller is to delay the onset of convection while maintaining a state of no motion in the fluid layer.

2. The mathematical model

Consider an infinite, horizontal liquid layer of thickness (d) bounded from below ($z = 0$) by an isothermal, solid surface at temperature, T_w. The other surface at $z = d$ is free, and it exchanges heat with a uniform temperature atmosphere at T_A. In the absence of motion, the temperature of the free surface is uniform at $T_A < T_F < T_w$ and the temperature gradient is perpendicular to the free surface (the Marangoni–Bénard problem). Heat is transmitted from the free surface to the atmosphere by Newton's law of cooling.

$$-\frac{\partial\theta}{\partial n} = Bi\theta \tag{1}$$

where $\theta = (T - T_A)/\beta d$ is the nondimensional temperature; n is a unit vector perpendicular to the free surface; $Bi = hd/k$ is the Biot number; h is a constant and uniform heat transfer coefficient; k is the liquid's thermal conductivity; and

$$\beta = \frac{T_w - T_F}{d} = \frac{Bi(T_w - T_A)}{d(1+Bi)} \tag{2}$$

is the opposite of the conductive temperature gradient.

The liquid is incompressible. The velocity vector, $\mathbf{u} = \{u, v, w\}$, satisfies the non-dimensional continuity equation,

$$\nabla\cdot\mathbf{u} = 0 \tag{3}$$

where u, v, w are the velocity components in the horizontal x and y, and the vertical z directions. κ/d is the velocity scale. $\kappa = k/(\rho C_p)$ is the thermal diffusivity. ρ and C_p are, respectively, the liquid's density and specific heat at constant pressure.

The non-dimensional momentum equation:

$$Pr^{-1}\left(\frac{\partial\mathbf{u}}{\partial t} + \mathbf{u}\cdot\nabla\mathbf{u}\right) = -\nabla p - F\hat{e}_z + \nabla^2\mathbf{u} \tag{4}$$

where p is the pressure. $Pr = \nu/\kappa$ is the Prandtl number. The time (t) scale is d^2/κ and the pressure scale is $\rho\kappa\nu/d^2$. $F = gd^3/(\nu\kappa)$ is the Galileo number. Buoyancy forces are neglected. The neglecting of buoyancy can be justified when either the layer is very thin or under microgravity conditions.

The energy equation is:

$$\frac{\partial\theta}{\partial t} + \mathbf{u}\cdot\nabla\theta = \nabla^2\theta. \tag{5}$$

The location of the perturbed free surface is given by

$$z = 1 + \eta(x, y, t). \tag{6}$$

The kinematic condition requires that the vertical component of the velocity, w, satisfies:

$$w = \left(\frac{\partial}{\partial t} + u\frac{\partial}{\partial x} + v\frac{\partial}{\partial y}\right)\eta. \tag{8}$$

In formulating the dynamic conditions at the interface, it is assumed that the overlying gas' viscosity can be neglected, the interface has negligible mass and the liquid properties at the interface are the same as the bulk liquid

properties. The non-dimensional surface tension (S) is expanded into a Taylor series in terms of the temperature,

$$S = C^{-1} - M\theta + \mathrm{O}(\theta^2) \tag{9}$$

where the surface tension was normalized using the group $\rho\nu\kappa/d$.

$$M = \left(-\frac{\mathrm{d}S^*}{\mathrm{d}T}\right)\frac{\beta d^2}{\rho\nu\kappa}$$

is the Marangoni number and S^* is the dimensional surface tension. $C = \rho\nu\kappa/(S_F^* d)$ is the crispation number. S_F^* and C^{-1} are, respectively, the dimensional and non-dimensional surface tensions at the conductive surface temperature, T_F.

The free surface stress conditions at $z = 1+\eta(x, y, t)$ are [19]:

$$\hat{n}\cdot\Gamma\cdot\hat{n} = 2H(C^{-1} - M\theta) \tag{10}$$

and

$$\tau^{(\alpha)}\cdot\Gamma\cdot\hat{n} = -\tau^{(\alpha)}M\nabla\theta. \tag{11}$$

In the above, H is the mean curvature of the interface,

$$2H = \left(\frac{\partial^2\eta}{\partial x^2}\left(1+\left(\frac{\partial\eta}{\partial y}\right)^2\right) + \frac{\partial^2\eta}{\partial y^2}\left(1+\left(\frac{\partial\eta}{\partial x}\right)^2\right)\right)\left(1+\left(\frac{\partial\eta}{\partial x}\right)^2+\left(\frac{\partial\eta}{\partial y}\right)^2\right)^{-3/2} \tag{12}$$

Γ is the stress tensor for an incompressible liquid,

$$\Gamma_{i,j} = -p\delta_{i,j} + \left(\frac{\partial u_i}{\partial x_j} + \frac{\partial u_j}{\partial x_i}\right) \tag{13}$$

and the indices 1, 2, and 3 denote respectively, the x, y and z directions. $\tau^{(\alpha)}$, $\alpha = 1, 2$, are orthonormal tangent vectors to the free surface.

In the classical Marangoni–Bénard problem, the boundary conditions at the solid surface, $z = 0$, are nonslip, $\mathbf{u} = 0$, and uniform temperature,

$$\theta(x, y, 0) = \frac{1+Bi}{Bi}. \tag{14}$$

Equations (1)–(14) admit the no-motion state,

$$\mathbf{u} = 0; \quad \theta(x, y, z) = \frac{1+Bi}{Bi} - z; \quad p = p_A + F(1-z) \tag{15}$$

where p_A is the nondimensional pressure of the atmosphere.

The linear stability of the no-motion state has been investigated by many researchers who computed the critical Marangoni number,

$$M_c = M(a, Bi, Bo, C) \tag{16}$$

where a is the wave number (which is defined later in the text) and

$$Bo = \frac{\rho g d_f^2}{S_0^*} = \frac{g d_f^3}{\nu\kappa}C$$

is the Bond number. When $M < M_c$, equation (15) is linearly stable. The objective of this paper is to demonstrate that with the use of feedback control strategies, it is possible to affect the stability characteristics of the no-motion state. In other words, we wish to maintain a stable no-motion state under conditions in which such a state would otherwise be nonstable.

3. The control strategy

In order to affect the stability of the fluid through the use of feedback control, it is envisioned that the solid surface is equipped with a large number of individually controlled actuators. Various types of actuators can be used. For instance, Tang and Bau [10] developed thermal actuators to stabilize the no-motion state of the Rayleigh–Bénard problem. One can also envision actuators that induce a vertical velocity component at the heated surface (i.e., suction and blowing).

Sensors detect the departure of the fluid from the desired, conductive state and they direct the actuators to take action so as to suppress unwanted disturbances. One can utilize a variety of sensors such as ones capable of detecting the shear stress at the solid surface, the level of the free surface, or the departure of the surface temperature from its conductive value. The latter two measurements can be carried out optically and non-intrusively. Since thermal actuation and optical sensing of surface temperature are relatively easy to implement, for concreteness, the discussion here focuses on these types of sensors and actuators. For simplicity, we assume that the sensors and actuators are continuously distributed and that each sensor directs an actuator installed directly beneath it at the same $\{x, y\}$ location. The sensor detects the deviation of the free surface temperature from its conductive value. The actuator modifies the heated surface temperature according to the rule:

$$\theta(x, y, 0, t) = \frac{1+Bi}{Bi} - K\left(\theta(x, y, 1, t) - \frac{1}{Bi}\right) \tag{17}$$

where K is the scalar controller gain. In general, $K = K_P + K_D\,\mathrm{d}/\mathrm{d}t + K_I\int_0^t \mathrm{d}t$ can be a proportional-differential-integral controller. Here, the focus is only on proportional control.

Equation (17) can be rewritten more conveniently as

$$\theta'(x, y, 0, t) = -K\theta'(x, y, 1, t) \tag{18}$$

where θ' is the deviation of the fluid's temperature from its conductive value.

The continuous distribution of the sensors and actuators is assumed for mathematical convenience, and it is not necessary for the practical application of the controller. For example, in their experimental and numerical work, using a finite number of discrete sensors and actuators, Tang and Bau [10, 11] succeeded in suppressing

Rayleigh–Bénard cells in an upright cylinder. It is likely that the same will be true for the case of the Marangoni–Bénard convection in a finite size container. Although in this paper the analysis is carried out for an infinite fluid layer, the results are likely to indicate what one might expect to observe when studying finite size containers.

The control strategy in equation (18) is not the only one possible. For example, one can envision control algorithms in which all the sensors communicate with all the actuators, i.e.,

$$\theta'(x,y,0,t) = -\iint_{x,y} K(x,y)\theta'(x,y,1,t)\,\mathrm{d}x\,\mathrm{d}y$$

where $K(x,y)$ is a periodic control gain function. However, since our objective is simply to demonstrate that the system can be controlled, the simpler control strategy, equation (18), in which K is a scalar will be used.

To understand how the controller operates, it is useful to review briefly the physical mechanisms that cause the Bénard–Marangoni instability. The no-motion state is an equilibrium state (a fixed point) of the uncontrolled system. Assume that as a result of a random disturbance, a hot spot is formed at some point on the free surface. Since (usually) the surface tension decreases with temperature, the surface tension at the hot spot location will be smaller than that at neighboring locations. As a result, there will be surface traction away from the hot spot, giving rise to a convective current. The convected fluid will be replaced by warmer fluid rising from beneath the surface.

For small Marangoni numbers, the convective motion is sufficiently slow to allow heat diffusion to equalize the rising fluid's temperature with that of its surroundings so as to remove the excess temperature and prevent the disturbance from manifesting itself. Under these conditions, the hot spot will eventually disappear and the no-motion state will be reinstated.

For supercritical Marangoni numbers, $M > M_c$, the disturbance-induced motion is sufficiently fast so that the heat dissipating mechanisms in the fluid do not have sufficient time to equilibrate the temperature of the rising fluid with its surroundings. As a result, the surface disturbance is manifested and convection will prevail.

Our controller acts to enhance the dissipative mechanisms in the fluid. The controller senses when a fluid column is about to rise and directs the actuator to drop slightly the heated surface temperature beneath the rising column. In turn, the rising column will carry less excess temperature than in the absence of the controller. As a result, the surface tension-induced currents will be weaker, allowing ample time for heat dissipation to equalize the surface temperature and restore the no-motion state. The control signal is proportional to the magnitude of the disturbances. When disturbances are small (infinitesimal), the modulations of the heated surface temperature will also be infinitesimal. In other words, the controller affects the dynamics of the system without significantly affecting the bottom surface temperature.

4. Linear stability of the controlled problem

Standard methods of linear stability analysis are used to determine the effect of the controller gain, K, on the critical Marangoni number at the onset of convection. The linear stability of the uncontrolled problem has attracted considerable attention in the literature. The linear stability of the no-motion state was first investigated by Pearson [20] who assumed an infinite fluid layer, a nondeformable surface, and zero gravity. The flat surface approximation is valid for a very large surface tension or in the asymptotic limit of $C \to 0$. Pearson demonstrated that there exists a critical Marangoni number, M_C, so that for $M < M_C$, the no-motion state is stable with respect to small disturbances. The magnitude of M_C depends on the heat transfer conditions (the Biot number) but not on the Prandtl number. For example, for an isothermal hot boundary and $Bi \to 0$, $M_C \sim 79.6$. Subsequently, using similar approximations to those used by Pearson, Nield [21] and Takashima [22] extended Pearson's analysis to include both buoyancy ($Ra > 0$) and surface tension effects (the Rayleigh–Bénard–Marangoni problem). In his work, Takashima [22] also accounted for heat conduction in the underlying solid plate. For $M > M_C$, time-independent motion sets up. We will refer to this convective motion as Pearson's modes.

In their analysis, both Pearson and Nield assumed that the loss of stability occurs through a real, simple eigenvalue (the principle of exchange of stability is valid). Unlike the case of the onset of convection in the Rayleigh–Bénard problem, the linearized operator of the Bénard–Marangoni problem is not self-adjoint and a rigorous proof of the validity of the principle of exchange of stability is yet to be found. Nevertheless, in extensive numerical experiments, Vidal and Acrivos [23] and Takashima [24] found that in all the cases investigated, when surface deformation was neglected ($C = 0$), the principle of exchange of stability was, indeed, valid.

The assumption of a non-deformable free surface was first relaxed by Scriven and Sternling [25] who accounted for capillary waves ($C > 0$) but not gravity waves ($Bo = 0$). Scriven and Sternling concluded that the critical Marangoni number $M_C \to 0$ as the disturbance wave number $a \to 0$. In other words, the no-motion state is always unstable to disturbances with a very long wavelength. In a confined medium, there will be a cut-off wave number (a_1) due to the restrictive effect of the confining boundaries that will lead to $M_C > 0$. Scriven and Sternling's analysis was modified by Smith [26] to include surface gravity waves which were shown to have a stabilizing effect. Smith showed that the values of M_C as

predicted by Pearson are valid for situations when the crispation number, C, is not large and $Bo > 0$. When $C > 0$, Takashima [27] and Gouesbet et al. [28] demonstrated that for layers heated from below ($M > 0$) the principle of exchange of stability is still valid. They found, however, onset of oscillatory convection for negative Marangoni numbers.

Here, similar ideas are extended to the controlled problem. The conservation equations and boundary conditions are linearized about the no-motion, conductive state. With the aid of a Taylor series expansion, the boundary conditions at the free interface are transformed to $z = 1$ and the uniform temperature boundary condition (14) at $z = 0$ is replaced with the controller rule, equation (18).

The vertical velocity and temperature are expanded into normal modes:

$$\begin{pmatrix} w(x,y,z) \\ \theta'(x,y,z) \\ \eta(x,y,t) \end{pmatrix} = \begin{pmatrix} W(z) \\ \Theta(z) \\ N \end{pmatrix} \exp(i(k_x x + k_y y) + \sigma t). \tag{19}$$

Upon substituting equation (19) into the linearized equations, we obtain a set of linear differential equations,

$$(\sigma Pr^{-1} - (D^2 - a^2))(D^2 - a^2) W = 0 \tag{20}$$

and

$$(\sigma - (D^2 - a^2))\Theta = W \tag{21}$$

where $a^2 = k_x^2 + k_y^2$ and the operator, $D = \mathrm{d}/\mathrm{d}z$. The boundary conditions are:

$$W(1) - \sigma N = 0 \tag{22}$$

$$C(Pr^{-1}\sigma - (D^2 - 3a^2))DW(1) + (Bo + a^2)a^2 N = 0 \tag{23}$$

$$((D^2 + a^2))W(1) + a^2 M(\Theta(1) - N) = 0 \tag{24}$$

$$(D + Bi)\Theta(1) - BiN = 0 \tag{25}$$

$$W(0) = DW(0) = 0 \tag{26}$$

and

$$\Theta(0) + K\Theta(1) = 0. \tag{27}$$

5. Stationary modes

In this section, it is assumed that the principle of exchange of stability is valid and that the bifurcation occurs from a conductive state to time-dependent convection. In other words, one can set $\sigma = 0$. Since in the uncontrolled case, the principle of exchange of stability is valid, this is also likely to be true for smaller controller gains. This, however, may not be the case for relatively large controller gains. The possible occurrence of a bifurcation into oscillatory convection (Hopf bifurcation) is addressed in the next section. The homogeneous equations (20)–(27) with $\sigma = 0$ constitute an eigenvalue problem for the critical Marangoni number. By substituting the general solution of equations (20) and (21) into the boundary conditions (22)–(27) and requiring the existence of nontrivial solutions, one obtains the critical Marangoni number:

$$M = \frac{4a(a^2 + Bo)(aK + a\cosh(a) + B_i \sinh(a))(2a - \sinh(2a))}{(a^2 + Bo)(a^3\cosh(a) - \sinh^3(a)) - 8a^5 C(K + \cosh(a))}. \tag{28}$$

The tedious task of carrying out the algebraic manipulation required to obtain equation (28) was greatly eased with the aid of Mathematica [29]. When one removes the feedback controller by setting $K = 0$, equation (28) reduces to the expression given by Takashima [26]. When one sets both $K = 0$ and $C = 0$, one obtains Pearson's [20] classical expression. When the principle of exchange of stability is valid, the critical Marangoni number is independent of the Prandtl number. Thus, the results of this section are applicable to all Prandtl numbers.

When $C < C^*$, where

$$C^* = \frac{(a^2 + Bo)}{16a^4 Bi}(\cosh(2a) - 1 - 2a^3 \coth(a)) \tag{29}$$

$(\partial M/\partial K)_{K=0} > 0$ and small controller gains have a stabilizing effect. When (a) is small, $C^* \approx a^2 Bo/(120Bi)$. As ($a$) increases so does C^* (monotonically). In other words, when $C = 0$, small controller gains always lead to an increase in the magnitude of M. When $C > 0$, there may be circumstances, in particular at small wave numbers (long wavelengths) in which the controller may have a destabilizing effect.

5.1. The effect of the controller on Pearson's modes (C = 0)

The Pearson modes evolve when no surface deformation occurs, i.e., the surface tension $S_0 \to \infty$ or the crispation number $C \to 0$. When $Bi = Bo = C = 0$, Fig. 1 depicts the critical Marangoni number at the onset of convection as a function of the wave number, a, for controller gains: $K = 0$, 5 and 20. When $C = 0$, the critical Marangoni number is infinity at $a = 0$. As a decreases, the Marangoni number decreases, attains a minimum at some critical wave number, and increases again.

In the absence of the controller, $K = 0$, the classical curve is reproduced and the critical Marangoni number attains the minimum of 79.6067 at $a = 1.993$. As the controller gain, K, increases, the marginal stability curves shift upwards, illustrating that the controller stabilizes the no-motion state for all wave numbers. The critical Marangoni number, $M_c = \mathrm{Min}_{a>0}(M)$, increases monotonically as the controller gain K increases. Figure 1 also illustrates that as K increases, the loss of stability occurs at larger wave numbers (shorter wavelengths). In

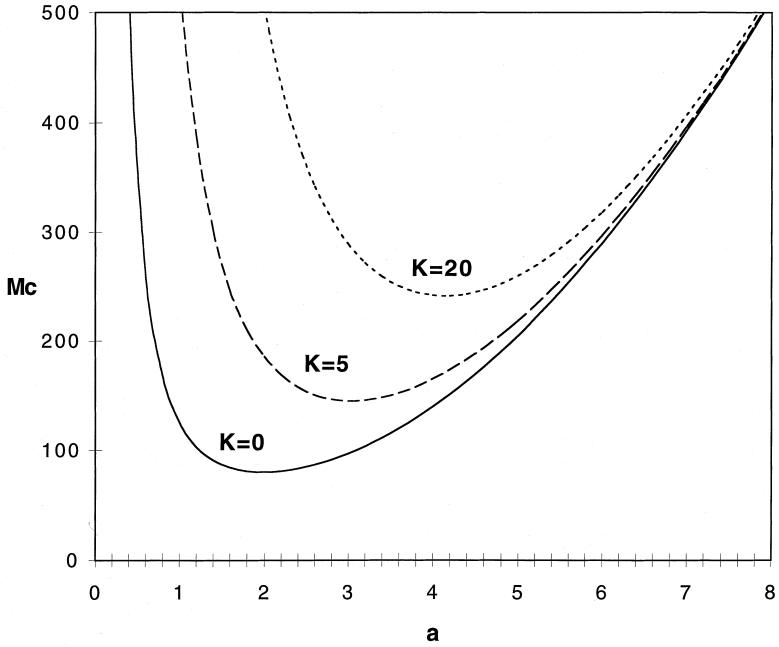

Fig. 1. The critical Marangoni number at the onset of convection is depicted as a function of the wave number, a, and controller gains: $K = 0$, 5 and 20; $Bi = Bo = C = 0$.

other words, the wave number that corresponds to the 'most dangerous' mode increases as the controller gain increases.

Figure 2 depicts the normalized critical Marangoni number, M_r, as a function of the controller gain for Biot numbers $Bi = 0$, 0.5 and 5. In Fig. 2, the Marangoni number was normalized with the critical Marangoni number in the absence of control and at the same Biot number, i.e.,

$$M_r = \frac{(M)_{\text{with control}}}{(M)_{\text{without control}}}.$$

For example, when $Bi = 5$, the Marangoni number was normalized with 250.6, which is the critical Marangoni number in the absence of control.

In the absence of control, the critical Marangoni number increases nearly linearly as the Biot number increases. This is because high Biot numbers provide a more efficient mechanism for the dissipation of thermal disturbances. As the Biot number increases, higher controller gains are needed to obtain the same relative change in the critical Marangoni number. For instance, when $Bi = 0$, a controller gain of 5 increases the critical Marangoni number from 79.6 ($K = 0$) to 144.7, a 182% increase. When $Bi = 1$, to increase the critical Marangoni number from 116.1 ($K = 0$) to 210.9, a 182% increase, a controller gain of 9.1 is needed.

In this subsection, it was demonstrated that in the case of the crispation number being equal to zero (the free interface remains flat), the controller can successfully suppress the Pearson modes and maintain a no-motion state under conditions in which, in the absence of the controller, motion would occur. In the next subsection, the requirement that $C = 0$ is relaxed and the case of a deforming interface is investigated.

5.2. C ≠ 0, Bo = 0

The case of $C > 0$ and Bond number, $Bo = 0$ (zero gravity), is investigated in this section. When $C = 0.001$, Fig. 3 depicts the critical Marangoni number at the onset of convection as a function of the wave number when the controller gains are $K = 0$, 5 and 10. In Fig. 3, $Bi = Bo = 0$. The situation here is significantly different than the case of $C = 0$ (Fig. 1). At $a = 0$ (very long wavelengths), the critical Marangoni number is zero. As a increases, the Marangoni number increases, attains a maximum, declines to a minimum and then increases again. For a truly infinite layer, the minimum of the Marangoni number is zero and a no-motion, conductive state does not exist. The controller is not effective at the wave number $a = 0$. In any practical situation, however, the layer will be confined in a finite size container, and very long wavelengths (small values of a) will not be admissible. In other words, in a confined container, the admissible wave numbers are restricted to some $a > a_1$, say, where the magnitude of a_1 depends on the geometry

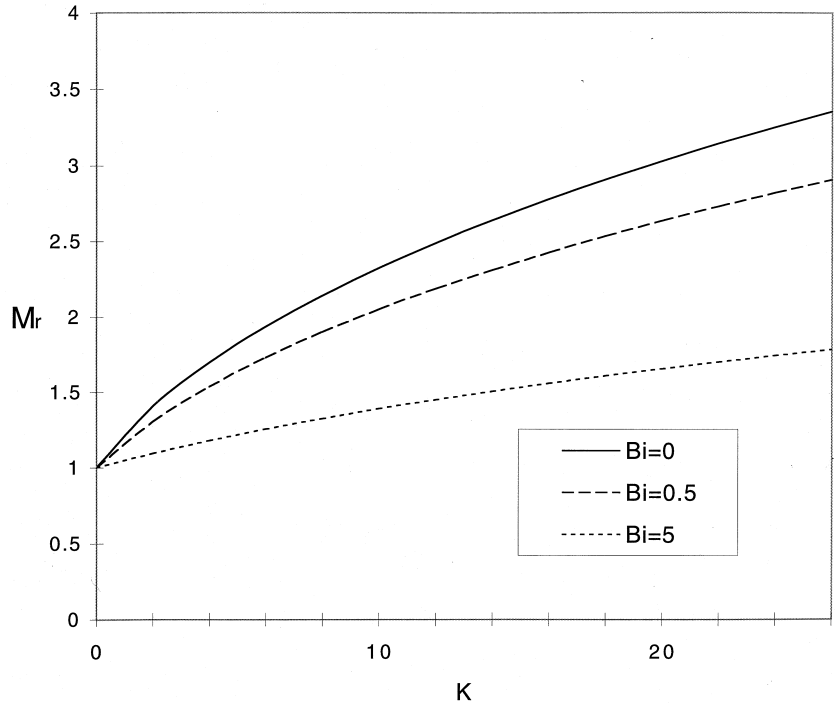

Fig. 2. The normalized Marangoni number is depicted as a function of the controller gain for $Bi = 0$, 0.5 and 5; $Bo = C = 0$.

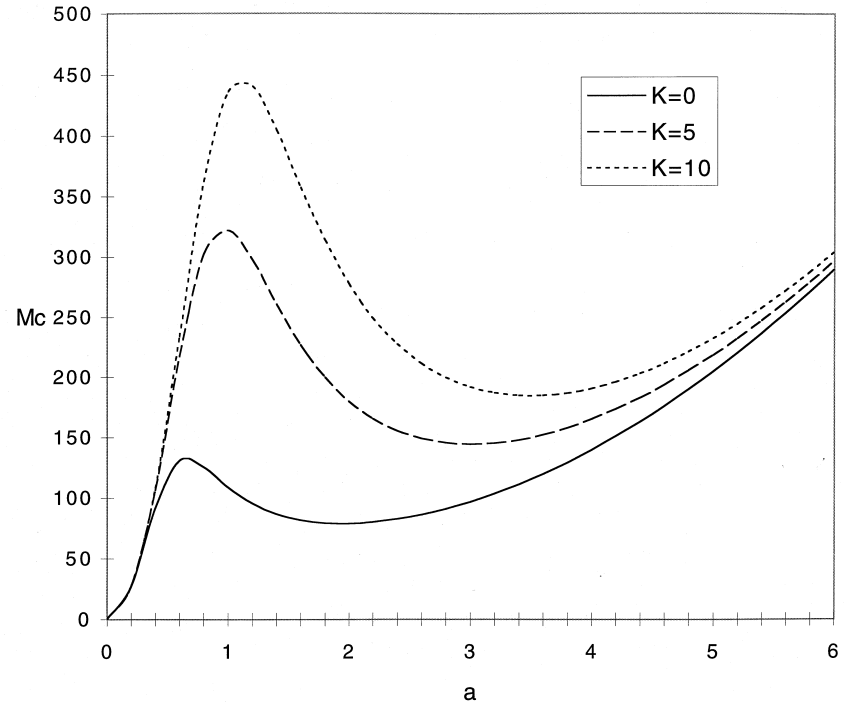

Fig. 3. The critical Marangoni number is depicted as a function of the wave number, a, for $K = 0$, 5 and 10; $Bi = Bo = 0$ and $C = 0.001$.

of the confining vessel. When $a > a_1 > 0$, the controller is effective, and it is capable of increasing the magnitude of the critical Marangoni number.

To examine more closely the dependence of the critical Marangoni number on a in the vicinity of $a = 0$, it is convenient to expand equation (28) into a Taylor series in terms of a, i.e.,

$$M \sim \left(\frac{2}{3}\right)\frac{Bo(1+Bi+K)}{C(1+K)} + \frac{\begin{pmatrix} C(120(1+Bi)+8Bo(3-2Bi)+K(120(2+Bi)+Bo \\ \times(48+44Bi))+24K^2(5+Bo))-Bo^2(1+Bi+K) \end{pmatrix}}{180C^2(1+K)^2}a^2 + O(a^4). \quad (30)$$

The series expansion reveals that when $Bo = 0$ and $C > 0$, M attains a zero value at $a = 0$. When $Bo = 0$ and $a > 0$, the controller is not effective. Moreover, when $Bo > 0$ and $Bi = 0$, the controller gain does not appear in the first term of the series expansion (30).

5.3. C > 0, Bo > 0

When $Bo > 0$, the critical Marangoni number at $a = 0$ is greater than zero. When the sign of the coefficient of the a^2 term in the Taylor series expansion (30) is positive, $a = 0$ corresponds to a local minimum of M. When the sign of the coefficient of the a^2 term in the Taylor series expansion (30) is negative, $a = 0$ corresponds to a local maximum of M. When

$$C \leqslant C_1 \equiv \frac{Bo^2(1+Bi+K)}{\begin{pmatrix} 4(30(1+Bi)+Bo(6-4Bi)+K(60+30Bi \\ +12Bo+11BiBo)+6K^2(Bo+5)) \end{pmatrix}} \quad (31)$$

the coefficient of a^2 is negative and the minimum of M occurs at $a > 0$. When $Bi = 0$,

$$C_1 = \frac{Bo^2}{24(5+Bo)(1+K)}.$$

When $Bi = 0.1$, $Bo = 0.1$ and $C = 10^{-4}$, Fig. 4 depicts the critical Marangoni number as a function of the wave number, a, for $K = 0$, 5 and 10. Witness that when $Bo > 0$, M no longer attains a zero value at $a = 0$. When $K = 0$, $C < C_1$ and $a = 0$ is not a local minimum. When $K = 5$ and 10, $C > C_1$ and $a = 0$ is a local (but not a global) minimum. In the vicinity of $a = 0$, an increase in the controller gain causes a decrease in the corresponding critical Marangoni number. When $a > a_1 > 0$, as the con-

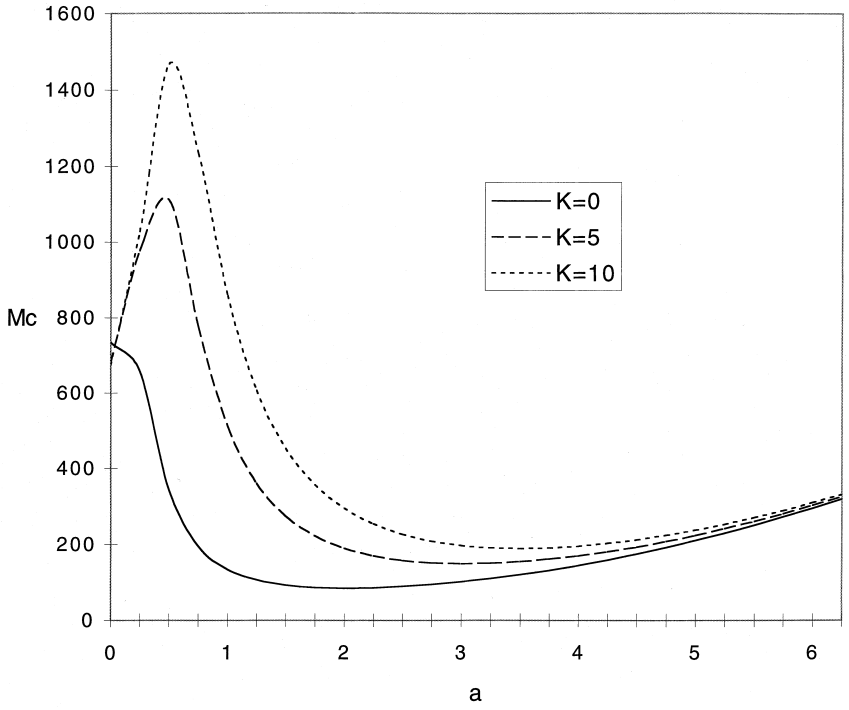

Fig. 4. The critical Marangoni number is depicted as a function of the wave number, a, for $K = 0$, 5 and 10; $Bi = 0.1$, $Bo = 0.1$ and $C = 10^{-4}$.

troller gain (K) increases, the curve shifts upwards and, most importantly, the controller increases the magnitude of the global minimum; thus it has a stabilizing effect.

6. Oscillatory modes

A general proof of the validity of the principle of exchange of stability is not available. Through extensive numerical experiments, Vidal and Acrivos [23] and Takashima [24, 27] demonstrated that in the uncontrolled case, the principle of exchange of stability holds for fluid layers heated from below. By continuity, one would expect that when the controller gains are small, the principle of exchange of stability will be preserved. Unfortunately, this may not be the case when the controller gains are not small. Large controller gains may induce oscillatory instabilities. In this section, the possibility of a bifurcation through an imaginary growth rate into oscillatory, time-dependent convection is briefly investigated.

For brevity's sake, only the case of $Pr \neq 1$ is considered here. Although straightforward, the expressions when $Pr = 1$ are different than those for $Pr \neq 1$ and for want of space are not reproduced here. The lack of an expression for $Pr = 1$ does not present a practical limitation since the expression given below can be used for values of Pr very close to one (i.e., $|Pr-1| > 0.01$).

The homogeneous equations (20)–(27) are solved when $\sigma \neq 0$. Again, the tedious algebraic manipulations were conveniently and efficiently carried out with the aid of Mathematica [29]. The existence of nontrivial solutions requires that the Marangoni number satisfy a characteristic equation of the form:

$$M = M_R + iM_I = -\frac{1}{a^2}\frac{\det(P)}{\det(Q)} \tag{32}$$

where M_R and M_I are real. For given Bi, Bo, C and K, both M_R and M_I are functions of the complex growth rate, $\sigma = \sigma_R + i\sigma_I$ and the wave number (a).

The components of the matrices P and Q are given below.

$$P_{1,1} = \frac{K}{\sigma}\left(\frac{\sinh(\sqrt{a^2+Pr^{-1}\sigma})}{1-Pr^{-1}} - \frac{\sqrt{a^2+Pr^{-1}\sigma}}{a}\sinh(a)\right)$$

$$P_{1,2} = \frac{1}{\sigma(Pr^{-1}-1)}(Pr^{-1}+K\cosh(\sqrt{a^2+Pr^{-1}\sigma}) + K(Pr^{-1}-1)\cosh(a))$$

$$P_{1,3} = K\sinh(\sqrt{a^2+\sigma})$$

$$P_{1,4} = 1+K\cosh(\sqrt{a^2+\sigma})$$

$$P_{2,1} = C\sqrt{a^2+Pr^{-1}\sigma}((2a^2+Pr^{-1}\sigma)\cosh(a) - 2a^2\cosh(\sqrt{a^2+Pr^{-1}\sigma})) + \frac{a}{\sigma}(a^2+Bo)(\sqrt{a^2+Pr^{-1}\sigma}\sinh(a) - a\sinh(\sqrt{a^2+Pr^{-1}\sigma}))$$

$$P_{2,2} = aC(\sqrt{a^2+Pr^{-1}\sigma}(2a\sqrt{a^2+Pr^{-1}\sigma} \times \sinh(\sqrt{a^2+Pr^{-1}\sigma}) - (2a^2+Pr^{-1}\sigma)\sin(a))) + \frac{a^2}{\sigma}((a^2+Bo)\cosh(\sqrt{a^2+Pr^{-1}\sigma}) - \cosh(a))$$

$$P_{2,3} = 0$$

$$P_{2,4} = 0$$

$$P_{3,1} = (2a^2+Pr^{-1}\sigma)\sinh(\sqrt{a^2+Pr^{-1}\sigma}) - 2a\sqrt{a^2+Pr^{-1}\sigma}\sinh(a)$$

$$P_{3,2} = -(2a^2+Pr^{-1}\sigma)\cosh(\sqrt{a^2+Pr^{-1}\sigma}) + 2a^2\cosh(a)$$

$$P_{3,3} = 0$$

$$P_{3,4} = 0$$

$$P_{4,1} = \frac{1}{(1-Pr^{-1})\sigma}(\sqrt{a^2+Pr^{-1}\sigma}(Pr^{-1}-1)\cosh(a) + \cosh(\sqrt{a^2+Pr^{-1}\sigma})) + B_iPr^{-1}\sinh(\sqrt{a^2+Pr^{-1}\sigma}))$$

$$P_{4,2} = \frac{1}{(Pr^{-1}-1)\sigma}(\sqrt{a^2+Pr^{-1}\sigma}\sinh(\sqrt{a^2+Pr^{-1}\sigma}) + a(Pr^{-1}-1)\sinh(a) + B_iPr^{-1}\cosh(\sqrt{a^2+Pr^{-1}\sigma}))$$

$$P_{4,3} = \sqrt{a^2+\sigma}\cosh(\sqrt{a^2+\sigma}) + Bi\sinh(\sqrt{a^2+\sigma})$$

$$P_{4,4} = \sqrt{a^2+\sigma}\sinh(\sqrt{a^2+\sigma}) + Bi\cosh(\sqrt{a^2+\sigma})$$

$$Q_{i,j} = P_{i,j} \quad (\{i = 1,2 \text{ and } 4\}, \{j = 1,2,3 \text{ and } 4\})$$

$$Q_{3,1} = \frac{Pr^{-1}}{(1-Pr^{-1})\sigma}\sinh(\sqrt{a^2+Pr^{-1}\sigma})$$

$$Q_{3,2} = \frac{Pr^{-1}}{(Pr^{-1}-1)\sigma}\cosh(\sqrt{a^2+Pr^{-1}\sigma})$$

$$Q_{3,3} = \sinh(\sqrt{a^2+Pr^{-1}\sigma})$$

and

$$Q_{3,4} = \cosh(\sqrt{a^2+Pr^{-1}\sigma}).$$

In the limit of $\sigma \to 0$, equation (32) reduces to equation

(28). In the limits of $\sigma \to 0$ and/or $a \to 0$, both the numerator and denominator of equation (32) approach zero and the numerical evaluation of equation (32) is susceptible to errors. To alleviate this problem, equation (32) was expanded into a Taylor series in terms of σ,

$$M = M_0 + \sigma M_1. \tag{33}$$

M_0 is the expression given in equation (28). Due to its length, M_1 is not reproduced here. When numerical values of M were needed for small values of σ, expression (33) was used instead of expression (32).

The admissible complex growth rates, σ, are located on the curve $M_I(\sigma) = 0$. The linear stability of the conductive state at any given Marangoni number, M, with respect to disturbances of wave number (a) is determined by the sign of the real part of σ obtained by solving the implicit equations, $M_R(a, \sigma_R, \sigma_I) = M$ and $M_I(a, \sigma_R, \sigma_I) = 0$.

The possible existence of $\{\sigma_R, \sigma_I\}$ pairs such that $M_I(a, \sigma_R, \sigma_I) = 0$ and $\sigma_I \neq 0$ was investigated. To this end, for various wave numbers (a), the curves $M_I(a, \sigma_R, \sigma_I) = 0$ in the σ_R–σ_I plane were plotted. When $K = Bi = Bo = C = 0$, the only curve satisfying $M_I(a, \sigma_R, \sigma_I) = 0$ corresponded to $\sigma_I = 0$. As the controller gain K was increased above zero, a second branch of $M_I(a, \sigma_R, \sigma_I) = 0$ that corresponds to $\sigma_I \neq 0$ appeared. For example, Fig. 5 depicts the locus of σ_R and $\sigma_I > 0$ that satisfy $M_I(a, \sigma_R, \sigma_I) = 0$ when $Bi = Bo = C = 0$, $Pr = 0.1$, $K = 5$ and $K = 20$ for wave numbers $a = 0.1$ and 1. A mirror image of the depicted curve exists (but is not shown) for $\sigma_I < 0$. The horizontal and vertical axes correspond, respectively, to σ_I and σ_R. The various points along the graph correspond to different values of the Marangoni number. A few values of M are indicated at various points along the $a = 1$ curve. Curves corresponding to $a > 1$ are located below the $a = 1$ curve. The $a = 0.1$ is located in close proximity to the $a = 0$ curve. When $K = 5$, although complex roots do exist, all of them have a negative real part. In other words, all the oscillatory modes decay in time.

As the controller gain, K, increases, the curves $M_I(a, \sigma_R, \sigma_I) = 0$ move upwards. Relatively large controller gains have a destabilizing effect as far as oscillatory modes are concerned. For example, controller gain $K = 20$ destabilizes the no-motion state and introduces oscillatory convection. Witness that even when $M = 0$, the real part of σ is positive and the no-motion state is non-stable with respect to oscillatory disturbances.

Similar plots of the locus of σ were prepared for other Prandtl numbers. Figure 6 depicts the locus of σ_R and $\sigma_I > 0$ that satisfy $M_I(a, \sigma_R, \sigma_I) = 0$ when $Bi = Bo = C = 0$, $Pr = 10$ and $K = 5$ for wave numbers $a = 0.1$ and 1. A mirror image of the depicted curve exists (but is not shown) for $\sigma_I < 0$. The various points along the graph correspond to different values of the Marangoni number. A few values of M are indicated at various points (solid circles) along the $a = 1$ curve (dashed line). On the curves, $\sigma_R < 0$ and the no-motion state is stable with respect to oscillatory modes.

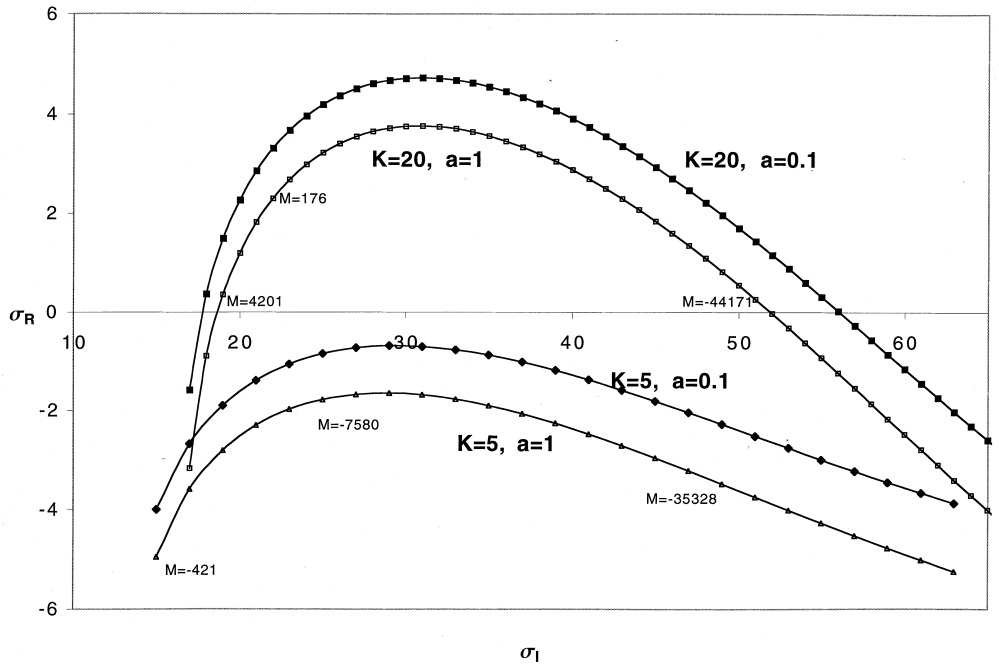

Fig. 5. The locus of σ_R and σ_I curves that satisfy $M_I(a, \sigma_R, \sigma_I) = 0$ is depicted in the σ_R–σ_I plane. $Bi = Bo = C = 0$, $Pr = 0.1$ and $K = 5$ and 20. Each point on the curve corresponds to a different Marangoni number.

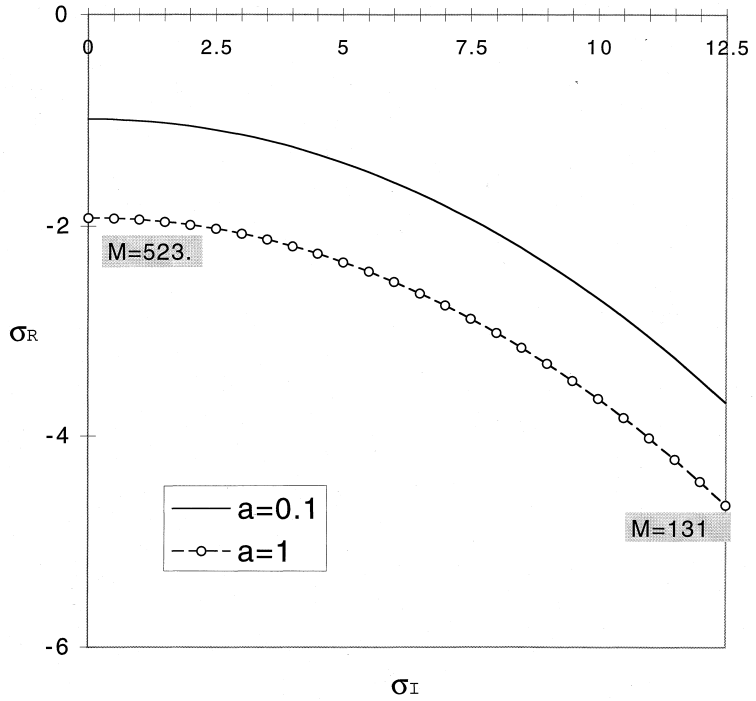

Fig. 6. The locus of σ_R and σ_I curves that satisfy $M_I(a, \sigma_R, \sigma_I) = 0$ is depicted in the σ_R–σ_I plane; $Bi = Bo = C = 0$, $Pr = 10$ and $K = 5$. Each point on the curve corresponds to a different Marangoni number.

Figures 5 and 6 illustrate that although in the presence of the controller, complex σ values are possible, as long as the controller gain is not too large, they all have a negative real part and the principle of exchange of stability is valid. As the wave number (a) decreases, the locus of admissible $\{\sigma_I, \sigma_R\}$ shifts upwards. This indicates that in the presence of the controller, disturbances with large wavelengths are less stable than disturbances with shorter wavelengths. In other words, oscillatory instability favors long wavelengths.

To further investigate the possible evolution of oscillatory instabilities, Figs 7 and 8 depict M_I as a function of σ_I when $Pr = 0.1$ and 10, respectively. In Figs 7 and 8, $Bi = Bo = C = \sigma_R = 0$. In Fig. 7, the wave number $a = 1.4$ and the controller gains are $K = 11$ (solid line) and 12 (dashed line). Similar curves were observed when $Pr < Pr^* \sim 1.1$. In Fig. 8, the wave number $a = 2$ and the controller gains are $K = 8$ (solid line) and $K = 10$ (dashed line). The admissible $\sigma_I - s$ correspond to $M_I = 0$. The curves always start at the origin ($\sigma_I = 0$, the case of exchange of stability). In order to obtain a bifurcation through an imaginary growth rate (oscillatory instability), the curves must intercept the $M_I = 0$ axis at $\sigma_I > 0$. For example, an oscillatory instability occurs in Fig. 7 when $K = 12$ but not when $K = 11$.

For any given controller gain (K), there is a critical wave number (a^*) above which oscillatory instabilities do not occur. The wave number a^* corresponds to the conditions when the local minimum of the curve is tangent to the $M_I = 0$ axis. For situations similar to the one depicted in Fig. 7 ($Pr < Pr^*$) the critical wave number, a^*, is determined by solving the simultaneous equations,

$$M_I(a^*, \sigma_I) = \frac{\partial M_I(a^*, \sigma_I)}{\partial \sigma_I} = 0 \tag{34}$$

for a^* and σ_I.

When $Pr > Pr^*$ (i.e., Fig. 8), the tangent occurs at $\sigma_I = 0$. In this case, $M_I(a^*, 0) = 0$ for all a^* and instead of using the derivative

$$\frac{\partial M_I(a^*, 0)}{\partial \sigma_I} = 0,$$

$$M_I(a^*, 0) = 0, \tag{35}$$

was used where M_I is the $O(\sigma_I)$ term in the Taylor series expansion of M, equation (33).

Figures 9 ($Pr = 0.1$) and 10 ($Pr = 10$) depict M_R as a function of the wave number (a) when $M_I = \sigma_R = 0$ and $Bi = Bo = C = 0$. The curves in Figs 9 and 10 depict the values of the Marangoni number at marginal stability.

Figure 9 ($Pr = 0.1$) depicts marginal stability curves when the controller gains are $K = 11.59$ (solid line) and $K = 11.8$ (dashed line). Similar curves were obtained

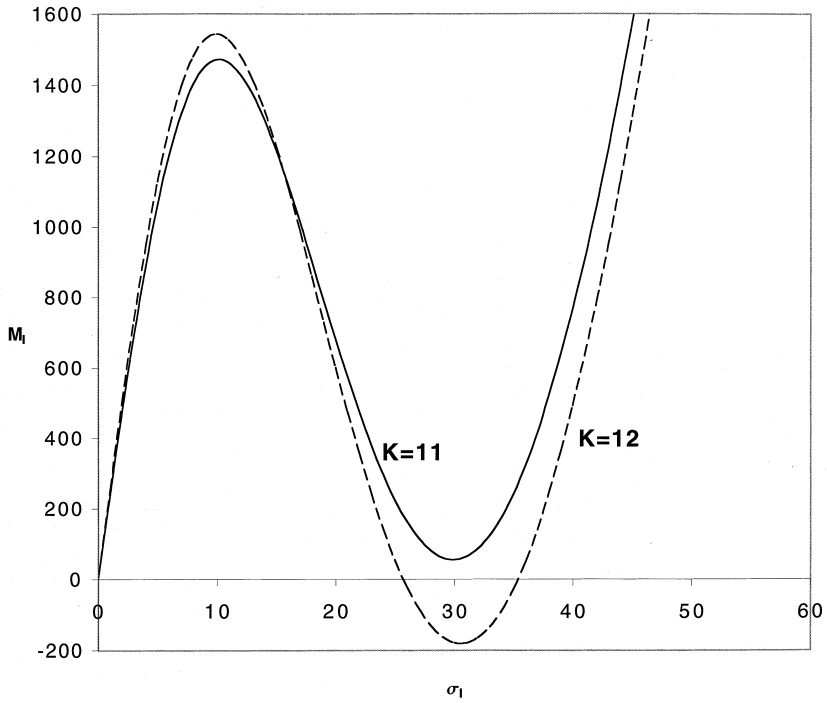

Fig. 7. $M_I(a, \sigma_R, \sigma_I)$ is depicted as a function of σ_I when $K = 11$ and 12; $Bi = Bo = C = \sigma_R = 0$, $a = 1.4$ and $Pr = 0.1$.

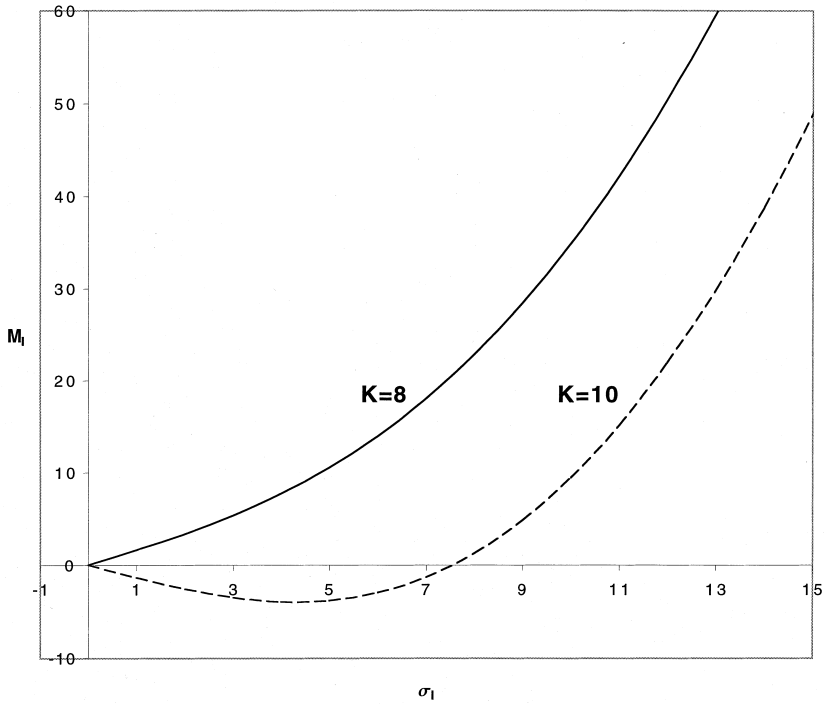

Fig. 8. $M_I(a, \sigma_R, \sigma_I)$ is depicted as a function of σ_I when $K = 8$ and 10; $Bi = Bo = C = \sigma_R = 0$, $a = 2$ and $Pr = 10$.

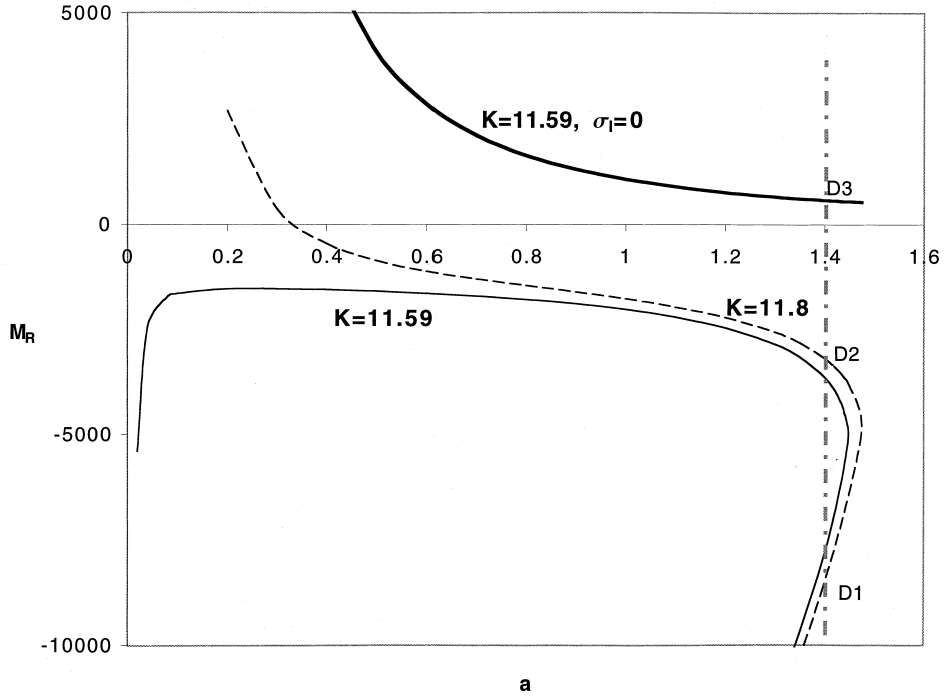

Fig. 9. When $K = 11.59$ (solid line) and 11.8 (dashed line), M_R is depicted as a function of the wave number (a). $M_I = \sigma_R = 0$ and $Bi = Bo = C = 0$, $Pr = 0.1$. The upper (heavy solid line) curve corresponds to exchange of stability ($\sigma_I = 0$) and $K = 11.59$. The lower curves correspond to bifurcation through imaginary growth rates ($\sigma_I \neq 0$).

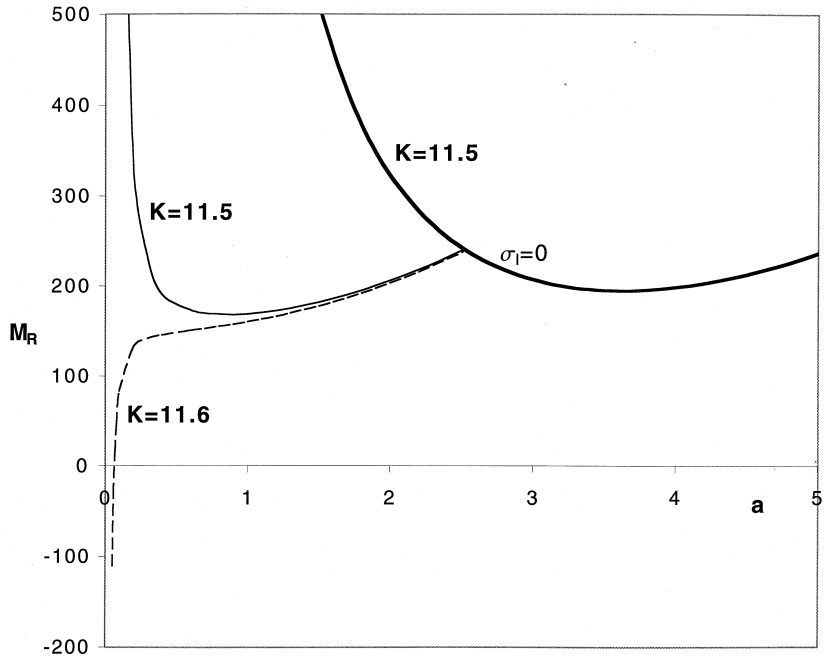

Fig. 10. When $K = 11.5$ (solid line) and 11.6 (dashed line), M_R is depicted as a function of the wave number (a). $M_I = \sigma_R = 0$ and $Bi = Bo = C = 0$; $Pr = 10$. The upper (heavy solid line) curve corresponds to exchange of stability ($\sigma_I = 0$) and $K = 11.59$. The lower curves correspond to bifurcation through imaginary growth rates ($\sigma_I \neq 0$).

when $Pr < Pr^*$. Witness the existence of two families of marginal stability curves. The upper (heavy solid line) curve corresponds to exchange of stability ($\sigma_I = 0$) and $K = 11.59$. The lower curves correspond to bifurcation through imaginary growth rates ($\sigma_I \neq 0$). To explain the significance of Fig. 9 the chain of events as the Marangoni number increases along the dashed, vertical line ($a = 14$) is described. The points D1, D2, and D3 denote the intersections of this line with the marginal stability curves. When the Marangoni number is negative and smaller than the value corresponding to point D1, the real part of the growth rate is negative and disturbances with wave number $a = 1.4$ decay. Along the segment D1–D2, the real part of the growth rate is positive and oscillatory disturbances with wave number $a = 1.4$ amplify. A negative Marangoni number occurs when the fluid layer is heated from above. The case of heating from above is not considered in this paper. As the Marangoni number increases above the value that corresponds to point D2, disturbances of wave number $a = 1.4$ decay. This situation persists until the Marangoni number is increased above the value corresponding to point D3. At D3, a non oscillatory loss of stability occurs. The critical Marangoni number corresponds to the global minimum of the marginal stability curves when $M_R > 0$. Figure 9 illustrates that when $K \leqslant 11.59$, the heavy solid line ($\sigma_I = 0$) determines the loss of stability and the principle of exchange of stability holds. When $K > 11.6$ (i.e., $K = 11.8$ in Fig. 9), the stability curve that corresponds to oscillatory modes crosses from the lower to the upper half plane and loss of stability occurs through a bifurcation into oscillatory modes. When $K > 11.6$, the no-motion state is unstable for all positive Marangoni numbers. The oscillatory destabilization occurs at smaller wave numbers (larger wavelengths) than in the case of exchange of stability.

An example of the stability diagram when $Pr > Pr^*$ is depicted in Fig. 10 for the case when $Pr = 10$. The heavy solid line depicts the marginal stability line for the case of exchange of stability ($\sigma_I = 0$) and $K = 11.5$. The light solid and dashed lines correspond to loss of stability through imaginary eigenvalues. When $Pr > Pr^*$, the marginal stability curve that corresponds to oscillatory modes bifurcates from the curve of exchange of stability (heavy solid line). At the intersection point between these two curves, $\sigma_I = 0$. The magnitude of σ_I increases as one moves away (to the left) from the intersection point. The critical Marangoni number is determined by the global minimum of these two curves. When $K = 11.5$, the global minimum corresponds to the oscillatory bifurcation, and it is lower ($M_c \sim 167$) than the minimum of the exchange of stability curve ($M \sim 195.3$, $a \sim 3.6$). In other words, when $K = 11.5$, oscillatory instability occurs at $M \sim 167$ and $a \sim 0.9$. To prevent the occurrence of the oscillatory instability one would need to reduce the controller gain. For example, when $K = 11$, the loss of stability occurs at $M = 191.4$ and $\sigma_I = 0$. The minimum of the oscillatory curve is then $M \sim 201.9$, which is larger than the global minimum. When the controller gain is increased to $K = 11.6$, the marginal stability curve turns down and crosses over to the lower half plane. When $K = 11.6$, oscillatory instabilities will manifest themselves even when $M = 0$. If one's objective is to stabilize the no-motion state, one would maintain $K < 11$.

Calculations similar to the ones depicted in Figs 9 and 10 were carried out for Prandtl numbers $0.1 \leqslant Pr \leqslant 10$ and $Bi = Bo = C = 0$. When $Pr < 10$ and $K < K_c \sim 11.6$, the principle of exchange of stability prevailed. When $Pr = 10$ and $K_1 < K < K_c$, where $K_1 \sim 11$, loss of stability occurred to oscillatory modes. When $K > K_c$ there is no critical Marangoni number and the no-motion state is unstable at all positive Marangoni numbers.

7. Conclusions

It has been demonstrated for the first time that the no-motion state in the Marangoni–Bénard problem can be controlled. Through the use of a simple control strategy, one can postpone the transition from the no-motion, conductive state to a time-independent motion. The controller delays loss of stability both in the case of a non-deforming surface (Pearson's modes) and in the case of a deforming surface when very long wavelengths are excluded. From a practical point of view, the exclusion of very long wavelengths may not pose a problem since such wavelengths may not be admissible in situations when the fluid is confined. When the controller gains are relatively large, the controller destabilizes the no-motion state and induces oscillatory convection. These oscillatory modes can perhaps be suppressed through the use of more sophisticated control strategies than the ones employed here. Moreover, it is likely that by optimizing the controller, one could maintain a no-motion state at higher Marangoni numbers than the ones reported here.

This paper focuses only on linear stability analysis, and it does not address the direction of the bifurcation and the basin of attraction of the controlled state. In some circumstances, it is possible that the loss of stability would occur through a subcritical bifurcation and that the basin of attraction of the controlled state will be limited. In other words, subcritical loss of stability may occur through finite amplitude disturbances. When a subcritical bifurcation occurs, a nonlinear controller can be used to render the subcritical bifurcation supercritical so as to prevent premature loss of stability. Yuen and Bau [4] demonstrated the feasibility of using such a nonlinear controller in the case of a simple convective system.

The analysis assumed that the sensors and actuators are continuously distributed. This may not be essential for the success of the controller. In their work on the

stabilization of Rayleigh–Bénard convection, Tang and Bau [11, 12] demonstrated, both in theory and experiment, that it is sufficient to use a finite number of sensors and actuators to successfully control the flow. Since on Earth Marangoni–Bénard convection is significant only for very thin layers in which the length scale of the convection is likely to be small, the actuators will need to be minute in size. Although microfabrication technology allows one to fabricate such actuators at a relatively low cost, the implementation of the controller may be expensive. The situation in microgravity is, however, quite different. In microgravity, in the absence of buoyancy, Marangoni convection plays an important role in deep fluid layers. Under these circumstances, the implementation of the proposed control strategy should be both feasible and beneficial. It is interesting to note that the same control strategy that delays the onset of Marangoni–Bénard convection is also effective in suppressing Rayleigh–Bénard convection.

Acknowledgement

This work was supported in part by grant CTS-9632237 from the National Science Foundation.

References

[1] J. Singer, Y.-Z. Wang, H.H. Bau, Controlling a chaotic system, Physical Review Letters 66 (1991a) 1123–1125.
[2] J. Singer, H.H. Bau, Active control of convection, Physics of Fluids A 3 (12) (1991b) 2859–2865.
[3] Y.-Z. Wang, J. Singer, H. H. Bau, Controlling chaos in a thermal convection loop, Journal of Fluid Mechanics 237 (1992) 479–498.
[4] P. Yuen, H.H. Bau, Rendering a subcritical bifurcation supercritical, Journal of Fluid Mechanics 317 (1996) 91–109.
[5] P. Yuen, H.H. Bau, Controlling chaotic convection using neural nets—theory and experiments, Neural Networks 11 (1998) 557–569.
[6] J. Tang, H.H. Bau, Stabilization of the no-motion state in Rayleigh–Bénard convection through the use of feedback control, Physical Review Letters 70 (1993a) 1795–1798.
[7] J. Tang, H.H. Bau, Feedback control stabilization of the no-motion state of a fluid confined in a horizontal, porous layer heated from below, Journal of Fluid Mechanics 257 (1993b) 485–505.
[8] J. Tang, H.H. Bau, Stabilization of the no-motion state in the Rayleigh–Bénard problem, Proceedings Royal Society A 447 (1994) 587–607.
[9] J. Tang, H.H. Bau, Stabilization of the no-motion state of a horizontal fluid layer heated from below with Joule heating, Trans. ASME Journal of Heat Transfer 117 (1995) 329–333.
[10] J. Tang, H.H. Bau, Experiments on the stabilization of the no-motion state of a fluid layer heated from below and cooled from above, Journal of Fluid Mechanics 363 (1998) 153–171.
[11] J. Tang, H.H. Bau, Numerical investigation of the stabilization of the no-motion state of a fluid layer heated from below and cooled from above, Physics of Fluids 10 (1998) 1597–1610.
[12] J. Tang, Active control of Rayleigh–Bénard convection, Ph.D. thesis, University of Pennsylvania, 1996.
[13] L.E. Howle, Control of Rayleigh–Bénard convection in a small aspect ratio container, International Journal of Heat and Mass Transfer 40 (1997) 817–822.
[14] L.E. Howle, Linear stability analysis of controlled Rayleigh–Bénard convection using shadowgraphic measurement, Physics of Fluids 9 (11) (1997) 3111–3113.
[15] L.E. Howle, Active control of Rayleigh–Bénard convection, Physics of Fluids 9 (7) (1997) 1861–1863.
[16] A.C. Or, R.E. Kelly, Onset of Marangoni convection in a layer of fluid modulated by a weak nonplanar oscillatory shear, International Journal of Heat and Mass Transfer 38 (12) (1995) 2269–2279.
[17] A.C. Or, R.E. Kelly, Thermocapillary and oscillatory shear instabilities in a layer of liquid with a deformable surface, Journal of Fluid Mechanics 360 (1998) 21–39.
[18] A.C. Or, R.E. Kelly, L. Cortelezzi, J.L. Speyer, Control of long wavelength Marangoni–Bénard convection (in review).
[19] S.H. Davis, Thermocapillary instabilities, Annual Review of Fluid Mechanics 19 (1987) 403–435.
[20] J.R.A. Pearson, On convection cells induced by surface tension, Journal of Fluid Mechanics 21 (1958) 489–500.
[21] D.A. Nield, Surface tension and buoyancy effects in cellular convection, Journal of Fluid Mechanics 19 (1964) 341–352.
[22] M. Takashima, Thermal instability of fluid layer bounded below by a solid layer of finite conductivity, Journal of the Physics Society of Japan 31 (1971) 283–292.
[23] A. Vidal, A. Acrivos, Nature of the neutral state in surface tension driven convection, Physics of Fluids 9 (1966) 615–616.
[24] M. Takashima, Nature of the neutral state in convective instability induced by surface tension and buoyancy, Journal of the Physics Society of Japan 28 (1970) 810.
[25] L.E. Scriven, C.V. Sterling, On cellular convection driven surface-tension gradients: effects of mean surface tension and surface viscosity, Journal of Fluid Mechanics 19 (1964) 321–340.
[26] M. Takashima, Surface tension driven instability in a horizontal liquid layer with a deformable free surface, I. Stationary convection, Journal of the Physics Society of Japan 50 (1981a) 2745–2750.
[27] M. Takashima, Surface tension driven instability in a horizontal liquid layer with a deformable free surface, II. Overstability, Journal of the Physics Society of Japan 50 (1981b) 2751–2756.
[28] G. Gouesbet, J. Maquet, C. Roze, R. Darrigo, Surface tension and coupled buoyancy-driven instability in a horizontal liquid layer—overstability and exchange of stability, Physics of Fluids A 2 (1990) 903–911.
[29] S. Wolfram, Mathematica, Cambridge, 1996.